Crystal structure of perfluorononanoic acid, $C_9HF_{17}O_2$

Joel W. Reid [1,a] Trimaan Malik,[2] Michael G. Pravica,[2] Adam F. G. Leontowich,[1] and Aly Rahemtulla[1]
[1]*Canadian Light Source, 44 Innovation Boulevard, Saskatoon, SK, Canada S7N 2V3*
[2]*Department of Physics and Astronomy, University of Nevada Las Vegas (UNLV), Las Vegas, NV 89154-4002, USA*

(Received 2 July 2024; accepted 6 August 2024)

The crystal structure of perfluorononanoic acid (PFNA) was solved via parallel tempering using synchrotron powder diffraction data obtained from the Brockhouse X-ray Diffraction and Scattering (BXDS) Wiggler Lower Energy (WLE) beamline at the Canadian Light Source. PFNA crystallizes in monoclinic space group $P2_1/c$ (#14) with lattice parameters $a = 26.172(1)$ Å, $b = 5.6345(2)$ Å, $c = 10.9501(4)$ Å, and $\beta = 98.752(2)°$. The crystal structure is composed of dimers, with pairs of PFNA molecules connected by hydrogen bonds via the carboxylic acid functional groups. The Rietveld-refined structure was compared to a density functional theory-optimized structure, and the root-mean-square Cartesian difference was larger than normally observed for correct powder structures. The powder data likely exhibited evidence of disorder which was not successfully modeled.

[doi:10.1017/S0885715624000356]

Key words: perfluorononanoic acid, PFNA, forever compounds, Rietveld refinement, density functional theory

I. INTRODUCTION

Perfluorononanoic acid (PFNA or $C_9HF_{17}O_2$, IUPAC name: heptadecafluorononanoic acid) is a compound belonging to the family of per- and polyfluoroalkyl substances (PFAS), characterized by alkyl chains decorated by fluorine atoms. Due to widespread industrial usage in diverse applications (surfactants, surface treatment agents for textiles, fire-fighting foams, and production of other fluorinated compounds, among others) and the strong nature of carbon-fluorine bonds making the compounds highly resistant to degradation, PFAS have become ubiquitous environmental contaminants (Dadashi Firouzjaei et al., 2022; Evich et al., 2022). PFAS have been implicated in numerous health concerns such as liver and kidney disease, reproductive and developmental issues, and cancer (Fenton et al., 2021), but due to the variety of different compounds (numbering in the thousands) and complexity of human population studies, much still remains unknown about their health effects (Kirk et al., 2018). PFNA is prominently included in a toxicology literature database with 29 common PFAS compounds (Pelch et al., 2022).

In this work, synchrotron powder X-ray diffraction (PXRD) data were obtained for PFNA and used to solve the crystal structure. Subsequent Rietveld refinement strongly suggested the presence of disorder which we were unable to model. A structureless Le Bail refinement was used to extract a complete Bragg reflection list unbiased by the structural model for inclusion in the Powder Diffraction File (Kabekkodu et al., 2024).

TABLE I. The crystal data, data collection, and refinement parameters obtained for monoclinic PFNA

Crystal data	
Formula, Z	$C_9HF_{17}O_2$, $Z = 4$
Molar mass	464.07 g/mol
Symmetry, space group	Monoclinic, $P2_1/c$ (#14)
Unit cell parameters	$a = 26.172(1)$ Å, $b = 5.6345(2)$ Å, $c = 10.9501(4)$ Å, $\beta = 98.752(2)°$
Volume	1596.0(1) Å^3
Density (ρ_{calc})	1.931 g/cm^3
Data Collection	
Beamline	CLS WLE
Monochromator	Si (111) single-bounce crystal monochromator
Detectors	8 Dectris Mythen2 X series 1 K strip detectors
Specimen mounting	1.2 mm inner diameter glass capillary
Collection mode	Transmission
Wavelength	$\lambda = 0.81906$Å
Refinement range	5°–40° (2θ)
Refinement	
Background correction	16-term log interpolation function
Number of data points	14 001
Number of restraints	81
Number of refined parameters	122
wR	0.0314
R_{wp}	0.0286
R_p	0.0170

[a]Author to whom correspondence should be addressed. Electronic mail: joel.reid@lightsource.ca

II. EXPERIMENTAL

A specimen of PFNA (Sigma-Aldrich, 97% purity) was lightly ground with a mortar and pestle, then inserted into a 1.2 mm inner diameter glass capillary for data collection.

PXRD data were collected using the Brockhouse X-ray Diffraction and Scattering sector Wiggler Low Energy (WLE) beamline (Leontowich et al., 2021) at the Canadian Light Source (CLS). WLE is an in-vacuum wiggler beamline which employs a Si (111) single-side bounce crystal monochromator. Data were collected at a photon energy of ~15.14 keV (calibrated wavelength of 0.81906Å), using a series of eight Dectris Mythen2 X series 1K strip detectors on the end of the goniometer arm (sample-detector distance of 767 mm). The precise wavelength and instrument resolution function were determined using Rietveld refinement of a pattern obtained from a lanthanum hexaboride (LaB_6) standard reference material (NIST SRM 660a LaB_6) using GSASII (Toby and Von Dreele, 2013). The sample was spun at 2 Hz during data acquisition.

Indexing of the PFNA pattern with DICVOL06 (Boultif and Louër, 2004) suggested a monoclinic unit cell with lattice parameters $a = 26.1585$ Å, $b = 5.6307$ Å, $c = 10.9423$ Å, $\beta = 98.759°$, and a cell volume of 1592.9 Å^3 ($M_{20} = 77.9$, $F_{20} = 418.7$). The cell volume was suitable for four formula units and space group determination with ChekCell (Laugier and Bochu, 2000) suggested $P2_1/c$ as the most likely space group. A PFNA molecule (minus the hydrogen atom) was obtained from the Cambridge Structural Database (Groom et al., 2016) entry KATVUY (Motreff et al., 2012), and then converted to a Fenske–Hall Z-matrix with Open Babel (O'Boyle et al., 2011). The Fenske–Hall Z-matrix with the PFNA molecule was uploaded into FOX (Favre-Nicolin and

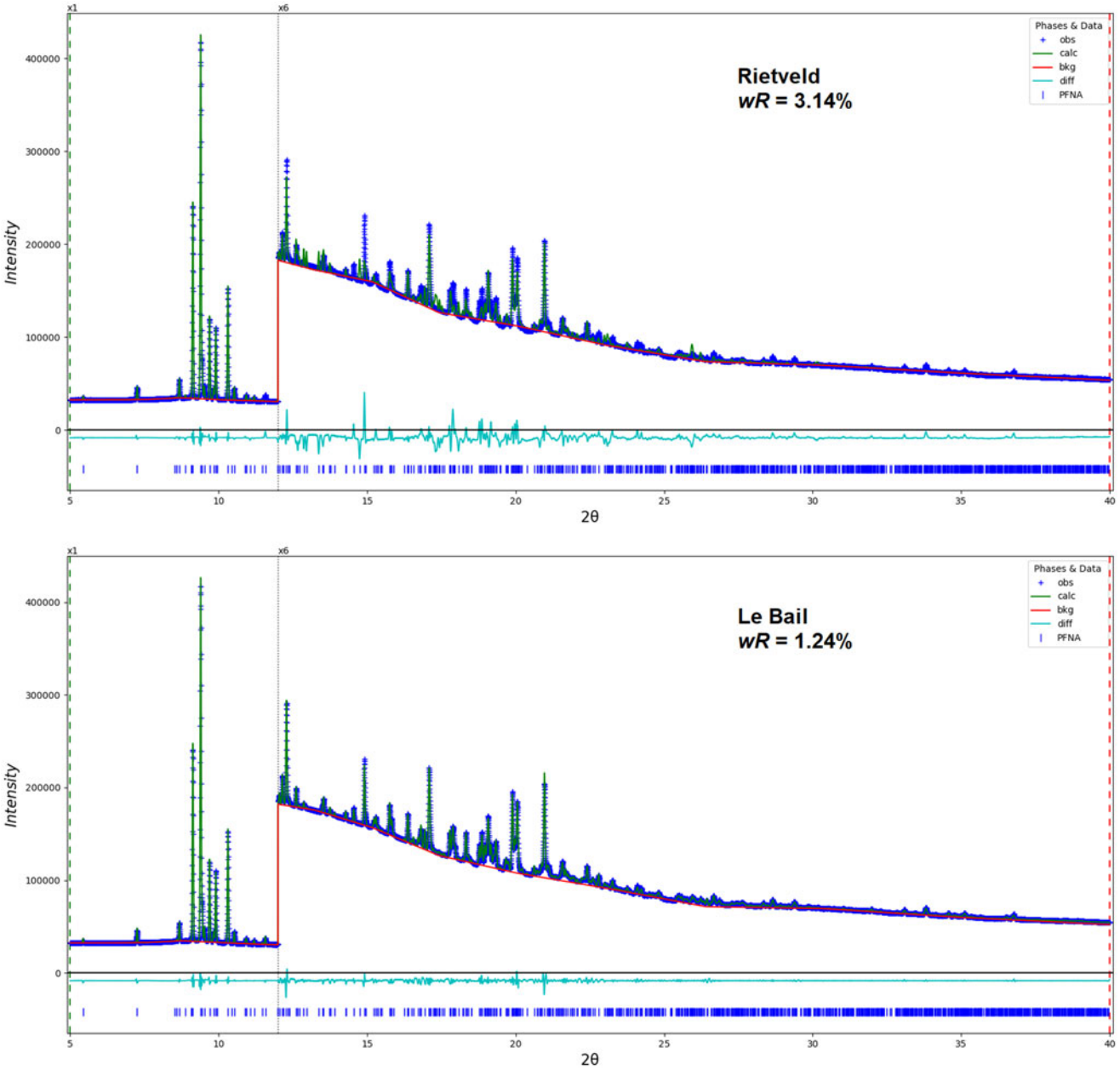

Figure 1. Plots illustrating the final Rietveld refinement ($wR = 3.14\%$, top) and Le Bail refinement ($wR = 1.24\%$, bottom) obtained for PFNA with GSASII. The region above 12° is magnified by 6× for each refinement to aid visualization.

https://doi.org/10.1017/S0885715624000356 Published online by Cambridge University Press

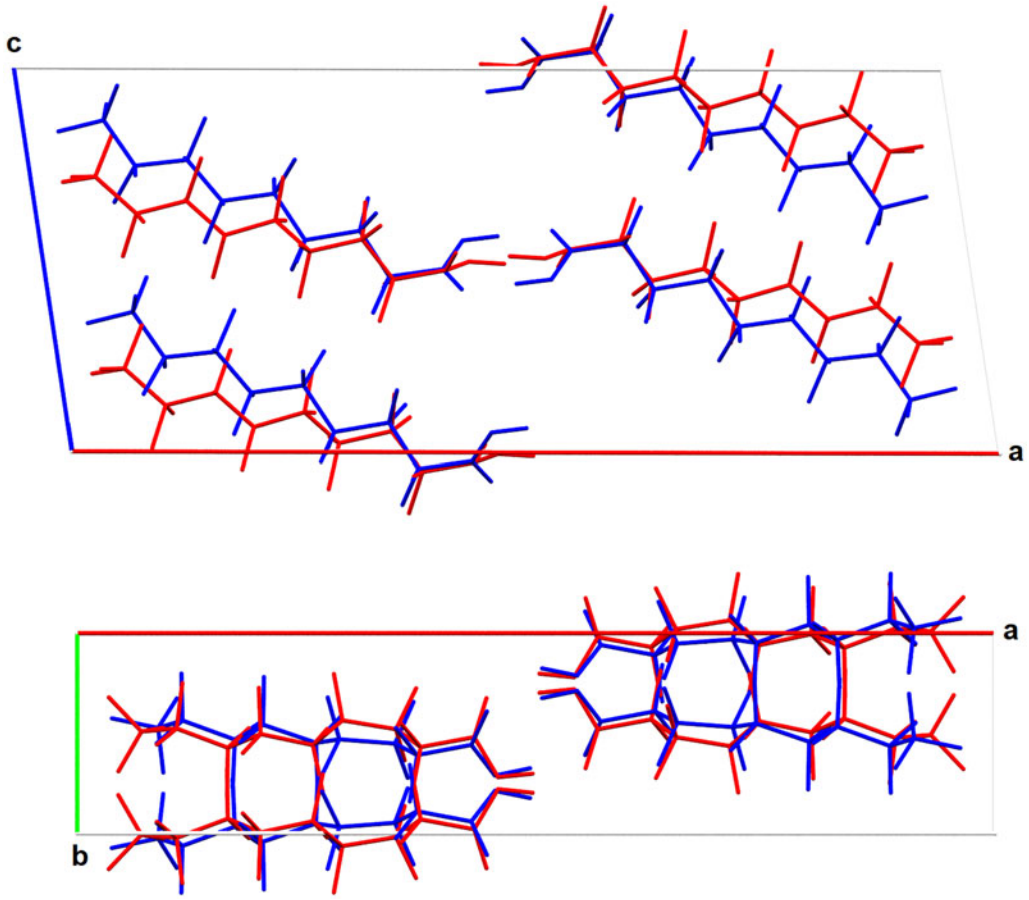

Figure 2. A comparison of the Rietveld-refined (red) and the DFT-optimized (blue) structures of PFNA, viewed along the *b*-axis (top) and the *c*-axis (bottom). The figure was prepared with Mercury (Macrae et al., 2008).

Černý, 2002) for structure solution with parallel tempering. Initial parallel tempering sets employing least-squares refinement every 250 000 trials were observed to significantly distort the PFNA molecule into unrealistic configurations. Subsequent parallel tempering sets employed rigid body constraints on the molecule without least-squares refinements, in order to find possible molecular packing arrangements without distorting the molecule. A number of different structures, including both dimers and columnar structures supporting zigzag chains of hydrogen bonds, were investigated with Rietveld refinement. Ultimately, a dimer structure was chosen based on the best fit to the data.

Rietveld refinement of the crystal structures was performed with the GSASII program (Toby and Von Dreele, 2013) using a Thompson–Cox–Hastings modified pseudo-Voigt peak shape function (Thompson et al., 1987). The background was modeled using a 16-term log interpolation function. Positional parameters were refined with restraints on bond distances and angles for all non-hydrogen atoms in the PFNA molecule obtained using Mogul (Bruno et al., 2004), with the mean and standard deviation quantities used to prepare the restraints. Individual isotropic displacement parameters were constrained to be the same for each element, with the value for the hydrogen atom constrained to be 1.3 times the value of the oxygen atoms. A fourth-order spherical harmonic texture model (Von Dreele, 1997) was used to correct for preferred orientation (PO), utilizing eight refined parameters.

The crystal data, data collection, and refinement details are summarized in Table I.

Density functional theory (DFT) geometry optimization was performed starting from the Rietveld-refined PFNA structure using CRYSTAL17 (Dovesi et al., 2018). Basis sets were obtained from the literature for the C, H, O (Gatti et al., 1994), and F atoms (Vilela Oliveira et al., 2019). The calculations used the B3LYP functional (Becke, 1993) and D3 dispersion correction (Grimme et al., 2010) with eight k-points.

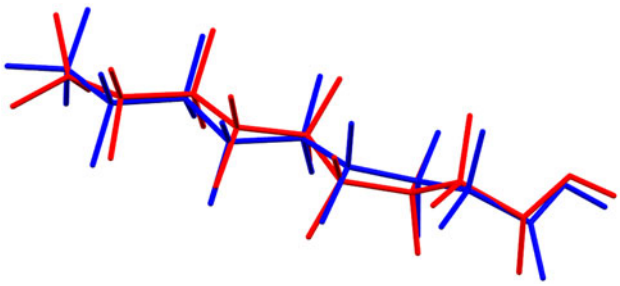

Figure 3. A comparison of the molecular overlay of the Rietveld-refined (red) and the DFT-optimized (blue) structures of PFNA obtained with Mercury (Macrae et al., 2008).

III. RESULTS AND DISCUSSION

The final Rietveld refinement obtained for the PFNA pattern is illustrated in Figure 1 (top), with the final Le Bail refinement (Figure 1, bottom) plotted below for comparison.

https://doi.org/10.1017/S0885715624000356 Published online by Cambridge University Press

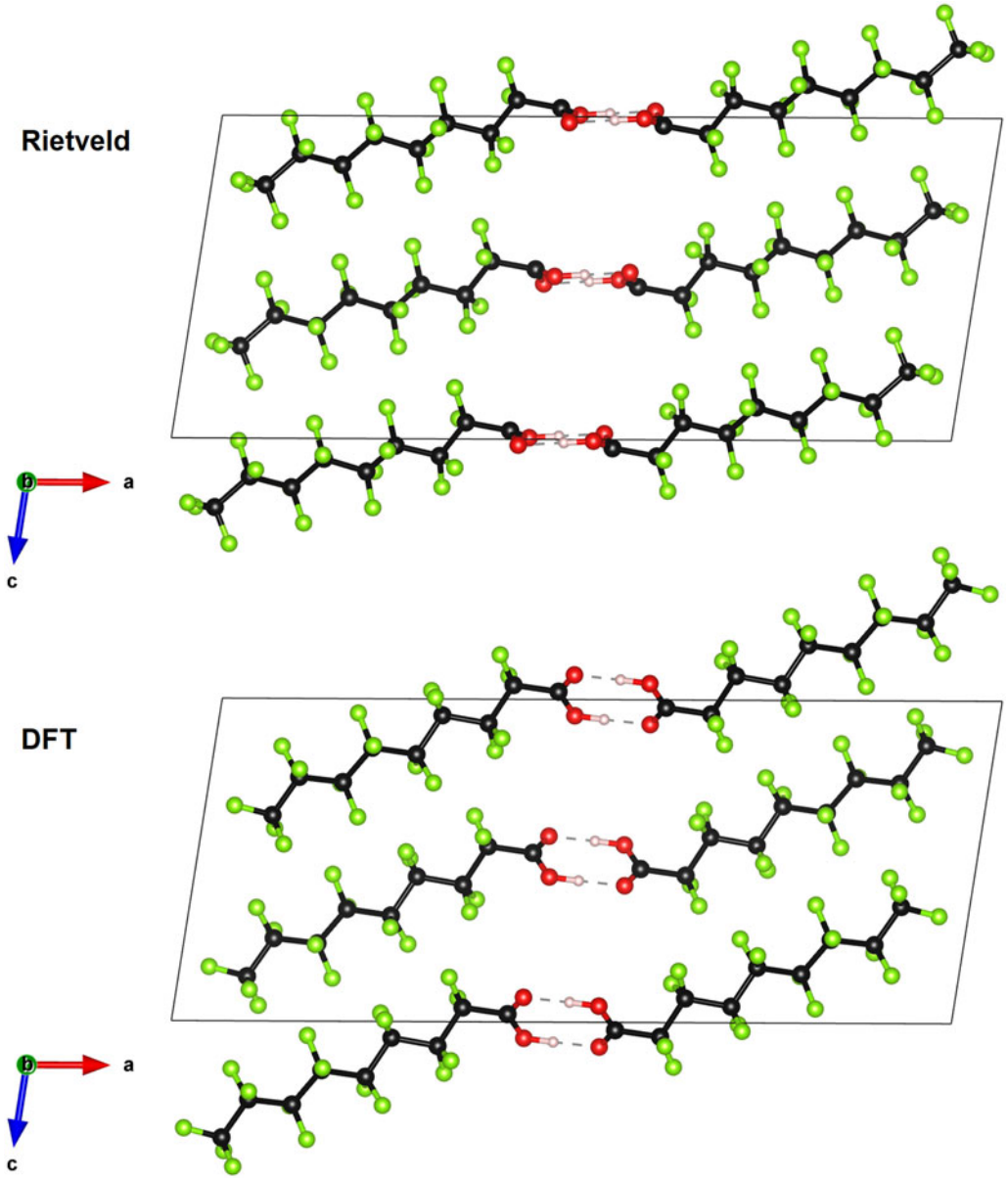

Figure 4. The Rietveld-refined (top) and DFT-optimized (bottom) crystal structure of PFNA, viewed along the *b*-axis. The atom types can be identified by color including carbon (black), fluorine (green), oxygen (red), and hydrogen (pink). Hydrogen bonds are represented by the dotted lines. The unit cell is outlined in black. The figure was prepared with VESTA (Momma and Izumi, 2011).

While the weighted R-factor is relatively low ($wR = 3.14\%$, which includes contributions of both the raw data points and the restraints) and the main features of the pattern are well described, discrepancies between observed and calculated peak intensities can be observed in the minor Bragg reflections. The weighted R-factor for the Le Bail refinement ($wR = 1.24\%$) is significantly lower, and visually the Le Bail fit is superior. The spherical harmonic PO correction yielded a texture index of 1.201(4) and improved the fit, but did not eliminate the discrepancies between the observed and calculated peak intensities in the Rietveld refinement.

The final Rietveld-refined structure (red) is compared to the DFT-optimized structure (blue) for PFNA in Figure 2. The structures are dimers where the carboxylic acid groups form pairs of hydrogen bonds between molecules. The fundamental dimer structure, monoclinic unit cell, and space group are reasonably consistent with the hydrogenated analog of PFNA, nonanoic acid ($C_9H_{18}O_2$), which was previously determined using single crystal data (Bond, 2004). While the Rietveld-refined and DFT-optimized structures are similar, there is clearly a shift in the position of the DFT-optimized molecule, which is more pronounced toward the trifluoromethyl end. The root-mean-squared (RMS) Cartesian displacement between the Rietveld-refined and the DFT-optimized structures for the non-hydrogen atoms is 1.12 Å, which falls outside the range generally expected for correct crystal structures using powder diffraction data (Van de Streek and Neumann, 2014). The RMS displacement obtained using the molecular overlay function of Mercury (Macrae et al., 2008) is 0.515 Å. Mercury performs a least-squares alignment of the two molecules, resulting in the improved agreement compared with the absolute Cartesian displacement. The molecular overlay of the Rietveld-refined and DFT-optimized molecules is illustrated in Figure 3 and

https://doi.org/10.1017/S0885715624000356 Published online by Cambridge University Press

TABLE II. The Rietveld-refined crystal structure of PFNA with lattice parameters $a = 26.172(1)$ Å, $b = 5.6345(2)$ Å, $c = 10.9501(4)$ Å, and $\beta = 98.752(2)°$.

Atom	*x/a*	*y/b*	*z/c*	U_{iso} (Å^2)
O1	0.45854(27)	−0.2198(22)	−0.0049(13)	0.236(7)
O2	0.44594(30)	0.1749(21)	0.0182(14)	0.236(7)
C3	0.43261(17)	−0.0196(18)	−0.0267(7)	0.192(5)
C4	0.37424(17)	−0.0692(12)	−0.0516(5)	0.192(5)
F5	0.3643(3)	−0.3115(14)	−0.0634(11)	0.2189(25)
F6	0.35297(30)	0.0472(20)	−0.1590(7)	0.2189(25)
C7	0.34734(21)	0.0201(12)	0.0528(5)	0.192(5)
F8	0.3692(4)	0.2240(16)	0.0885(9)	0.2189(25)
F9	0.3567(4)	−0.1357(20)	0.1489(8)	0.2189(25)
C10	0.28893(22)	0.0641(13)	0.0215(5)	0.192(5)
F11	0.2796(4)	0.2963(15)	0.0373(9)	0.2189(25)
F12	0.2704(4)	−0.0062(20)	−0.0967(7)	0.2189(25)
C13	0.25679(23)	−0.0594(14)	0.1018(5)	0.192(5)
F14	0.2723(4)	0.0217(22)	0.2139(7)	0.2189(25)
F15	0.2674(4)	−0.2938(16)	0.1008(9)	0.2189(25)
C16	0.19973(24)	−0.0043(13)	0.0629(5)	0.192(5)
F17	0.1804(4)	−0.0990(18)	−0.0467(7)	0.2189(25)
F18	0.1978(4)	0.2268(15)	0.0512(9)	0.2189(25)
C19	0.16399(24)	−0.0726(12)	0.1517(6)	0.192(5)
F20	0.1631(4)	−0.3176(14)	0.1538(9)	0.2189(25)
F21	0.1868(4)	0.0243(18)	0.2623(7)	0.2189(25)
C22	0.10816(23)	0.0234(13)	0.1185(6)	0.192(5)
F23	0.1144(4)	0.2502(14)	0.0979(10)	0.2189(25)
F24	0.0867(4)	−0.0565(18)	0.0076(7)	0.2189(25)
C25	0.06970(23)	0.0085(14)	0.2142(5)	0.192(5)
F26	0.0447(4)	−0.1903(16)	0.2127(9)	0.2189(25)
F27	0.0342(4)	0.1793(17)	0.2005(9)	0.2189(25)
F28	0.0952(4)	0.0281(19)	0.3265(7)	0.2189(25)
H29	0.49617	−0.2022	−0.0102	0.307(9)

All atoms belong on Wyckoff 4e sites and were refined with fixed site occupancies of 1.

differences are observed, particularly with respect to the trifluoromethyl and carboxylic acid orientations at the ends of the molecules. Despite restraints, the intermolecular hydrogen bonds formed between the carboxylic acid groups are shorter in the Rietveld-refined structure (H29···O2 = 1.539(6) Å) than in the DFT-optimized structure (H29···O2 = 1.60 Å). The eight-atom ring formed by the two hydrogen-bonded carboxylic acid groups is also perfectly planar in the DFT-optimized structure, but slightly irregular in the Rietveld-refined structure, as illustrated in Figure 4. Arguably, the most unusual features of the experimental structure are the torsion angles about the C7–C10 axis (four torsion angles based on two fluorine atoms per carbon atom). These torsion angles fall outside the distributions given by Mogul for similar geometries. Calculation of the powder pattern using the DFT-optimized structure results in significantly different pattern intensities than the experimental pattern, suggesting it is somewhat different than the true experimental structure. The Rietveld-refined atomic coordinates are given in Table II, and the atomic labels used in the refinement are illustrated in Figure 5. The largest peak and hole in the difference Fourier map for the Rietveld-refined structure were 0.67 and −0.83 eÅ^{-3}, respectively.

Given the plausibility of the refined structure and the relatively large isotropic displacement parameters observed (see Table II), disorder was considered as a possible reason for the discrepancies between the Rietveld and Le Bail refinements. Disorder can be observed in long-chain molecular structures; for example, the structure of Teflon, $(C_2F_4)_n$, can be disordered (Sprik et al., 1999). In an (unsuccessful) attempt to model the disorder, a structure solution was performed with FOX using two PFNA molecules with half occupancy to ascertain if a plausible overlapping structure with partial occupancies could be found. Despite running over 50 sets of parallel tempering, no plausible structures were observed with this approach, but this may be asking too much of the data.

In addition to the dimer structure, Rietveld refinement was performed on a columnar structure composed of double columns of PFNA molecules running parallel to the *b*-axis, with the molecules oriented perpendicular to the *b*-axis. The double columns were held together by a zig-zag ladder of hydrogen bonds. While the structure appeared plausible, the refinement was inferior to that obtained for the final dimer structure, and a DFT-optimization of the Rietveld-refined columnar structure failed to converge.

The most similar-length fluorinated compound to PFNA observed in the Cambridge Structural Database (CSD) is perfluorooctanoic acid (PFOA or $C_8HF_{15}O_2$) contained in CSD entry KEQREG (Omorodion et al., 2018). PFOA crystallizes in a significantly different structure with triclinic symmetry, composed of single columns of PFOA molecules running parallel to the *a*-axis. Each column is held together by a chain of hydrogen bonds connecting carboxylic acid groups of adjacent molecules in the column.

The Hirshfeld surface (Hirshfeld, 1977; Spackman and Byrom, 1997) of the PFNA molecule obtained using Crystal

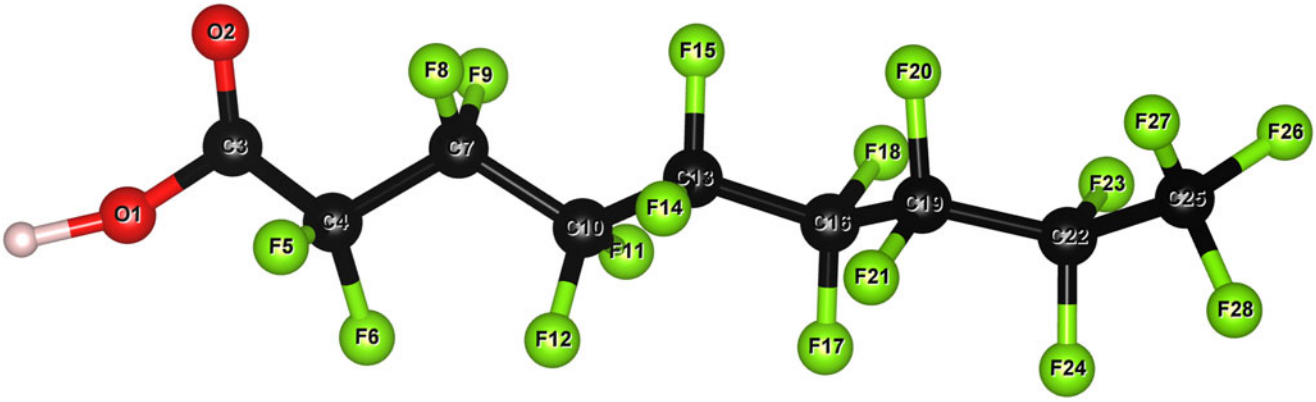

Figure 5. The atom labels used for the PFNA structure.

https://doi.org/10.1017/S0885715624000356 Published online by Cambridge University Press

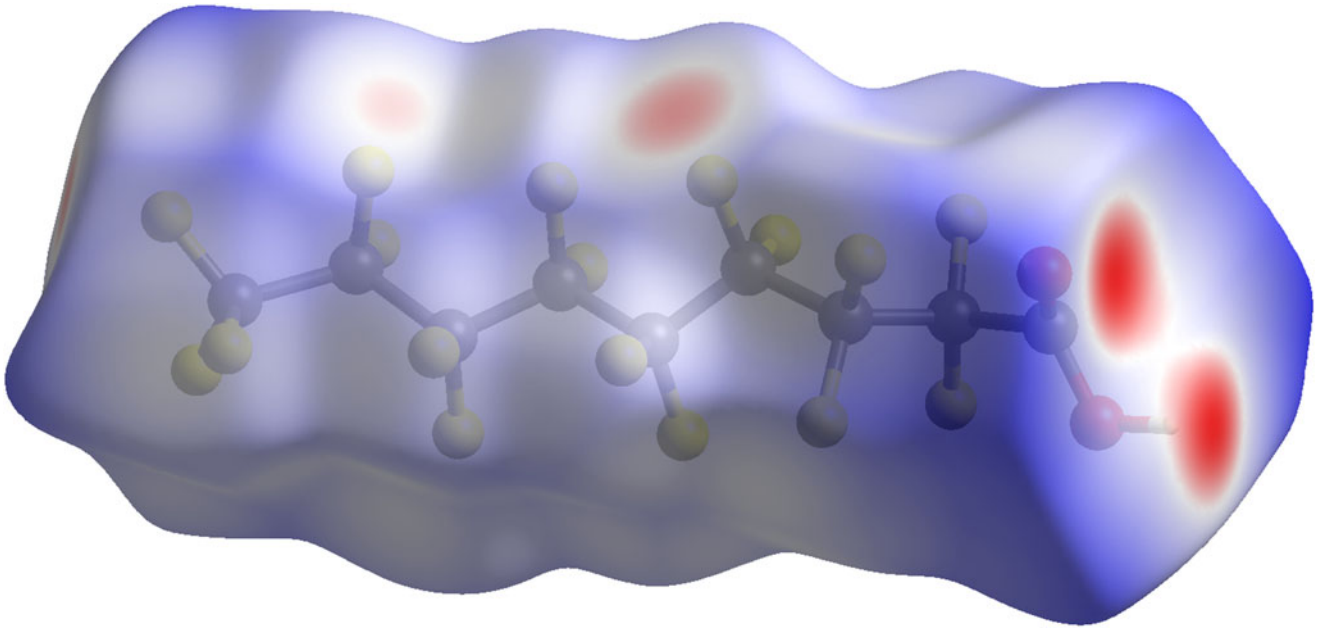

Figure 6. The Hirshfeld surface of PFNA. Regions in red represent intermolecular contacts shorter than the sum of the van der Waals radii, while regions in blue represent longer contacts and regions in white represent contacts equal to the sum of the van der Waal radii. The figure was prepared with Crystal Explorer (Spackman et al., 2021).

Explorer (Spackman et al., 2021) is illustrated in Figure 6. The volume enclosed within the Hirshfeld surface (395.08 $Å^3$) represents 99.0% of one-fourth of the unit cell volume, suggesting that the molecules are not tightly packed.

A Bragg reflection list for PFNA based on Le Bail refinement was prepared by summing reflections closer than 0.02°, 2θ as multiple reflections and assigning a weighted average reflection position, then including all reflections with relative integrated intensities of 0.2% or greater, up to 25° in 2θ.

IV. DEPOSITED DATA

Individual Crystallographic Information Framework (CIF) files containing the results of the final Rietveld refinement (crystal structure), Le Bail refinement (raw data and Bragg reflection list), and DFT-optimized structure were deposited with ICDD. The data can be requested at pdj@icdd.com.

ACKNOWLEDGEMENTS

JR would like to thank Jim Kaduk and Denis Spasyuk for helpful discussions regarding the crystal structure and suggestions which significantly improved the paper. MP and TM would like to acknowledge support from: (i) Gregory Holmbeck at Idaho National Laboratory through a Laboratory Directed Research & Development (LDRD) Program under U.S. Department of Energy (DOE) Idaho Operations Office Contract DE-AC07-05ID14517; and (ii) the U. S. DOE Office of Science Basic Energy Sciences program under Award Number DE-SC0023248.

Research described in this paper was performed using the WLE beamline at the Canadian Light Source, which is supported by the Canadian Foundation for Innovation, the Natural Sciences and Engineering Research Council of Canada, the National Research Council Canada, the Canadian Institutes of Health Research, the Government of Saskatchewan, Western Economic Diversification Canada, and the University of Saskatchewan.

CONFLICTS OF INTEREST

The authors have no conflicts of interest to declare.

REFERENCES

Becke, A. 1993. "Density-Functional Thermochemistry. III. The Role of Exact Exchange." *Journal of Chemical Physics* 98: 5648–52.

Bond, A. D. 2004. "On the Crystal Structures and Melting Point Alternation of the n-Alkyl Carboxylic Acids." *New Journal of Chemistry* 28 (1): 104–14.

Boultif, A., and D. Louër. 2004. "Powder Pattern Indexing with the Dichotomy Method." *Journal of Applied Crystallography* 37 (5): 724–31.

Bruno, I. J., J. C. Cole, M. Kessler, J. Luo, W. D. S. Motherwell, L. H. Purkis, B. R. Smith, R. Taylor, R. I. Cooper, S. E. Harris, and A. G. Orpen. 2004. "Retrieval of Crystallographically-Sderived Molecular Geometry Information." *Journal of Chemical Information and Computer Sciences* 44 (6): 2133–44.

Dadashi Firouzjaei, M., E. Zolghadr, S. Ahmadalipour, N. Taghvaei, F. A. Afkhami, S. Nejati, and M. A. Elliott. 2022. "Chemistry, Abundance, Detection and Treatment of Per-and Polyfluoroalkyl Substances in Water: A Review." *Environmental Chemistry Letters* 20 (1): 661–79.

Dovesi, R., A. Erba, R. Orlando, C. M. Zicovich-Wilson, B. Civalleri, L. Maschio, M. Rérat, S. Casassa, J. Baima, S. Salustro, and B. Kirtman. 2018. "Quantum-Mechanical Condensed Matter Simulations with CRYSTAL." *Wiley Interdisciplinary Reviews: Computational Molecular Science* 8 (4): e1360.

Evich, M. G., M. J. B. Davis, J. P. McCord, B. Acrey, J. A. Awkerman, D. R. U. Knappe, A. B. Lindstrom, T. F. Speth, C. Tebes-Stevens, M. J. Strynar, Z. Wang, E. J. Weber, W. M. Henderson, and J. W. Washington. 2022. "Per-and Polyfluoroalkyl Substances in the Environment." *Science* 375 (6580): eabg9065.

Favre-Nicolin, V., and R. Černý. 2002. "FOX, 'Free Objects for Crystallography': A Modular Approach to Ab Initio Structure Determination From Powder Diffraction." *Journal of Applied Crystallography* 35 (6): 734–43.

https://doi.org/10.1017/S0885715624000356 Published online by Cambridge University Press

Fenton, S. E., A. Ducatman, A. Boobis, J. C. DeWitt, C. Lau, C. Ng, J. S. Smith, and S. M. Roberts. 2021. "Per-and Polyfluoroalkyl Substance Toxicity and Human Health Review: Current State of Knowledge and Strategies for Informing Future Research." *Environmental Toxicology and Chemistry* 40 (3): 606–30.

Gatti, C., V. R. Saunders, and C. Roetti. 1994. "Crystal Field Effects on the Topological Properties of the Electron Density in Molecular Crystals: The Case of Urea." *The Journal of Chemical Physics* 101 (12): 10686–96.

Grimme, S., J. Antony, S. Ehrlich, and H. Krieg. 2010. "A Consistent and Accurate Ab Initio Parametrization of Density Functional Dispersion Correction (DFT-D) for the 94 Elements H-Pu." *The Journal of Chemical Physics* 132 (15): 154104

Groom, C. R., I. J. Bruno, M. P. Lightfoot, and S. C. Ward. 2016. "The Cambridge Structural Database." *Acta Crystallographica Section B: Structural Science, Crystal Engineering and Materials* 72 (2): 171–9.

Hirshfeld, F. L. 1977. "Bonded-Atom Fragments for Describing Molecular Charge Densities." *Theoretica Chimica Acta* 44: 129–38.

Kabekkodu, S. N., A. Dosen, and T. N. Blanton. 2024. "PDF-5+: a Comprehensive Powder Diffraction File™ for Materials Characterization." *Powder Diffraction*. in press.

Kirk, M., K. Smurthwaite, J. Braunig, S. Trevenar, C. D'Este, R. Lucas, A. Lal, R. Korda, A. Clements, J. Mueller, and B. Armstrong. 2018. *The PFAS Health Study: Systematic Literature Review*. Canberra: The Australian National University.

Laugier, J., and B. Bochu. 2000 "LMGP-Suite of Programs for the Interpretation of X-ray Experiments, ENSP/Laboratoire des Matériaux et du Génie Physique, BP 46, 38042 Saint Martin d'Hères, France.".

Leontowich, A. F. G., A. Gomez, B. D. Moreno, D. Muir, D. Spasyuk, G. King, J. W. Reid, C.-Y. Kim, and S. Kycia. 2021. "The Lower Energy Diffraction and Scattering Side-Bounce Beamline for Materials Science at the Canadian Light Source." *Journal of Synchrotron Radiation* 28 (3): 961–9.

Macrae, C. F., I. J. Bruno, J. A. Chisholm, P. R. Edgington, P. McCabe, E. Pidcock, L. Rodriguez-Monge, R. Taylor, J. V. D. Streek, and P. A. Wood. 2008. "Mercury CSD 2.0–New Features for the Visualization and Investigation of Crystal Structures." *Journal of Applied Crystallography* 41 (2): 466–70.

Momma, K., and F. Izumi. 2011. "VESTA 3 for Three-Dimensional Visualization of Crystal, Volumetric and Morphology Data." *Journal of Applied Crystallography* 44 (6): 1272–6.

Motreff, A., R. C. da Costa, H. Allouchi, M. Duttine, C. Mathonière, C. Duboc, and J.-M. Vincent. 2012. "A Fluorous Copper (II)–Carboxylate Complex Which Magnetically and Reversibly Responds to Humidity in the Solid State." *Journal of Fluorine Chemistry* 134: 49–55.

O'Boyle, N. M., M. Banck, C. A. James, C. Morley, T. Vandermeersch, and G. R. Hutchison. 2011. "Open Babel: An open chemical Toolbox." *Journal of Cheminformatics* 3: 1–14.

Omorodion, H., M. Palenzuela, M. Ruether, B. Twamley, J. A. Platts, and R. J. Baker. 2018. "A Rationally Designed Perfluorinated Host for the Extraction of PFOA From Water Utilising Non-Covalent Interactions." *New Journal of Chemistry* 42 (10): 7956–68.

Pelch, K. E., A. Reade, C. F. Kwiatkowski, F. M. Merced-Nieves, H. Cavalier, K. Schultz, T. Wolffe, and J. Varshavsky. 2022. "The PFAS-Tox Database: A Systematic Evidence Map of Health Studies on 29 Per-and Polyfluoroalkyl Substances." *Environment International* 167: 107408.

Spackman, M. A., and P. G. Byrom. 1997. "A Novel Definition of a Molecule in a Crystal." *Chemical Physics Letters* 267 (3-4): 215–20.

Spackman, P. R., M. J. Turner, J. J. McKinnon, S. K. Wolff, D. J. Grimwood, D. Jayatilaka, and M. A. Spackman. 2021. "Crystalexplorer: A Program for Hirshfeld Surface Analysis, Visualization and Quantitative Analysis of Molecular Crystals." *Journal of Applied Crystallography* 54 (3): 1006–11.

Sprik, M., U. Roethlisberger, and M. L. Klein. 1999. "Conformational and Orientational Order and Disorder in Solid Polytetrafluoroethylene." *Molecular Physics* 97 (3): 355–73.

Thompson, P., D. E. Cox, and J. B. Hastings. 1987. "Rietveld Refinement of Debye–Scherrer Synchrotron X-Ray Data from Al_2O_3." *Journal of Applied Crystallography* 20 (2): 79–83.

Toby, B. H., and R. B. Von Dreele. 2013. "GSAS-II: the Genesis of a Modern Open-Source All-Purpose Crystallography Software Package." *Journal of Applied Crystallography* 46 (2): 544–9.

Van de Streek, J., and M. A. Neumann. 2014. "Validation of Molecular Crystal Structures From Powder Diffraction Data with Dispersion-Corrected Density Functional Theory (DFT-D)." *Acta Crystallographica Section B: Structural Science, Crystal Engineering and Materials* 70 (6): 1020–32.

Vilela Oliveira, D., J. Laun, M. F. Peintinger, and T. Bredow. 2019. "BSSE-Correction Scheme for Consistent Gaussian Basis Sets of Double-and Triple-Zeta Valence With Polarization Quality for Solid-State Calculations." *Journal of Computational Chemistry* 40 (27): 2364–76.

Von Dreele, R. B. 1997. "Quantitative Texture Analysis by Rietveld Refinement." *Journal of Applied Crystallography* 30 (4): 517–25.

https://doi.org/10.1017/S0885715624000356 Published online by Cambridge University Press